HAL
archives-ouvertes.fr

Nanohybrids with magnetic and persistent luminescence properties for cell labelling, tracking, in vivo real-time imaging and magnetic vectorization

E Teston, T Maldiney, I Marangon, J Volatron, Y. Lalatonne, L. Motte, C Boisson-Vidal, G. Autret, O Clément, D. Scherman, et al.

▶ **To cite this version:**

E Teston, T Maldiney, I Marangon, J Volatron, Y. Lalatonne, et al.. Nanohybrids with magnetic and persistent luminescence properties for cell labelling, tracking, in vivo real-time imaging and magnetic vectorization. Small, Wiley-VCH Verlag, 2018. hal-02325611

HAL Id: hal-02325611
https://hal.archives-ouvertes.fr/hal-02325611

Submitted on 22 Oct 2019

HAL is a multi-disciplinary open access archive for the deposit and dissemination of scientific research documents, whether they are published or not. The documents may come from teaching and research institutions in France or abroad, or from public or private research centers.

L'archive ouverte pluridisciplinaire **HAL**, est destinée au dépôt et à la diffusion de documents scientifiques de niveau recherche, publiés ou non, émanant des établissements d'enseignement et de recherche français ou étrangers, des laboratoires publics ou privés.

Nanohybrids with magnetic and persistent luminescence properties for cell labelling, tracking, *in vivo* real-time imaging and magnetic vectorization

E. Teston, T. Maldiney, I. Marangon, J. Volatron, Y. Lalatonne, L. Motte, C. Boisson-Vidal, G. Autret, O. Clément, D. Scherman, F. Gazeau, C. Richard

Dr E. Teston, Dr. T. Maldiney, Prof. D. Scherman, Dr. C. Richard, Unité des Technologies Chimiques et Biologiques pour la Santé (UTCBS), UMR 8258 CNRS, U 1022 Inserm, Faculté de Pharmacie de Paris, F-75270 cedex France, Chimie Paristech, Paris F-75231 cedex France. cyrille.richard@parisdescartes.fr

Dr. I. Marangon, J. Volatron, Dr. F. Gazeau, Laboratoire Matière et Systèmes Complexes (MSC), UMR 7057 CNRS, Université Paris Diderot, Paris 75205 cedex, France

Dr. Y. Lalatonne, Prof. L. Motte, Laboratoire de Chimie, Structures, Propriétés de Biomatériaux et d'Agents Thérapeutiques (CSPBAT), UMR 7244 CNRS, Université Paris, Bobigny, 93017, France,

Dr C. Boisson-Vidal, Unité mixte de recherche 1140 - Thérapeutiques innovantes en hémostase, Faculté de Pharmacie de Paris, F-75270 cedex France,

Dr. G. Autret, Prof. O. Clément, Laboratoire de Recherche en Imagerie, EA 4062, Inserm U 970 ou 494, Equipe 2, PARCC, Université Paris Descartes, Hôpital Européen George Pompidou, Paris 75015, France

Abstract:

Once injected into a living organism, cells diffuse or migrate around the initial injection point and become impossible to be visualized and tracked *in vivo*. The present work concerns the development of a new technique for therapeutic cell labelling and subsequent *in vivo* visualisation and magnetic retention. We hypothesized and subsequently demonstrated that nanohybrids made of persistent luminescence nanoparticles (PLNPs) and ultrasmall superparamagnetic iron oxide nanoparticles (USPIOs) incorporated into a silica matrix can be used as an effective nanoplatform to label therapeutic cells in a non-toxic way in order to dynamically track them in real-time *in vitro* and in living mouse. As a proof-of-concept, we have shown that once injected, these labelled cells could be visualized and attracted *in vivo* using a magnet. This first step suggests that our nanohybrids represent efficient multifunctional nanoprobes for further imaging guided cell therapies development.

1) Introduction

In recent years, cells have shown great potential in a number of biomedical applications and researches in this area received much attention.[1] Cell therapies using mesenchymal stem cells (MSC) or endothelial progenitor cells (EPC) have demonstrated significant potential for the treatment and cure of several diseases such as cancer, diabetes, neurodegenerative or cardiovascular diseases[2-4] and also for regeneration in peripheral arterial disease (PAD) in both animal and human studies.[5-6]

Most current preclinical and clinical cell therapy trials consist of local or systemic delivery of stem or progenitor cells, and rely on the migration and retention of implanted cells at sites of

injury.[7] However, determining the fate and localization of these cells inside the body, as well as targeting the cells to a particular location, are still major challenges. To address these concerns, several methods have been developed to label therapeutic cells *ex vivo* in order to monitor their fate after *in vivo* administration. Among the different available modalities, X-ray computed tomography (CT),[8] magnetic resonance imaging (MRI),[9] positron emission tomography (PET)[10] and single photon emission computed tomography (SPECT)[11] have been used. However, the detection sensitivity of transplanted cells using such techniques is in some cases very low, or rendered difficult and costly by the use of radiopharmaceutical compounds. Optical imaging is expected to contribute to the development of cell transplantation, as it is less costly, easier to handle, non-ionizing and very sensitive.[12] For that purpose, various optical labelling techniques have been developed to apprehend cell behavior *in vitro* and *in vivo*.[13] However, optical *in vivo* detection is impaired by the autofluorescence signal coming from the body when exciting the probes.[14] To overcome this parasitic signal, our group pioneered the use of persistent luminescent nanoparticles (PLNPs) for *in vivo* imaging. Acting as optical capacitors, PLNPs can emit light in the tissue transparency window for minutes to hours after the end of an UV or visible illumination, leading to signals without autofluorescence and high target to background ratio.[15-20] Recently, ultrasensitive detection of labelled cells in small animals either after intravenous (IV) or subcutaneous (SC) injection was demonstrated in preliminary studies using PLNPs.[18,21-22]

The long-term efficacy of stem cells therapy is presently relatively low, which can be due to a lack of cell retention in the treatment area,[23] misplaced-injection, or cell injection into highly fibrotic tissues.[24] Fortunately, unproperly localized injection can be prevented by real-time imaging guidance to ensure sufficient cell delivery to the desired tissue location. In order to improve cell delivery, several reports have shown that the *in vivo* biodistribution of cells

labelled with magnetic nanoparticles could be influenced by applying a magnetic field and gradient.[25-26] Various preclinical studies have exploited the magnetic properties acquired by cells carrying magnetic nanoparticles in order to increase the retention of implanted cells at specific sites within the body, for example with endothelial cells or EPC.[27-30]

Recently, we have developed a modified approach to synthesize a new class of mesoporous nanohybrids (MPNHs) consisting of PLNPs and USPIOs incorporated into the same mesoporous silica matrix.[31] We thus wondered whether these new nanohybrids could be used to label cells of interest in order to both control their *in vivo* fate, using their magnetic property, and to follow in real-time their distribution, using their persistent luminescent property, after injection. As a model, we chose a subpopulation of EPC called "late" EPC or endothelial colony-forming cells (ECFC) that present blood vessel-forming ability.[32-33] Herein, we report the use of MPNHs to label ECFC in non-toxic conditions, allowing these cells to keep their proliferation ability and biological properties. After labelling, it was possible to detect the cells *in vivo* and we show that MPNHs-COOH labelled ECFC can be remotely controlled *in vivo* by applying an external magnetic field and gradient.

2. Results and discussion

2.1. Characterization and functionalization of the nanohybrids

We have previously reported the synthesis of different mesoporous nanohybrids (MPNH) made of PLNPs and containing increasing amount of USPIOs (0, 1.4, 3.5 and 5.2% (w/w), named $MPNH_0$, $MPNH_1$, $MPNH_2$ and $MPNH_3$, respectively) incorporated into a silica matrix (Fig 1.a-d). These nanohybrids have been synthesized using tetraethoxysilane (TEOS), cetyltrimethylammonium bromide (CTAB) and comprise the two types of nanoparticles (PLNPs and USPIOs).[31] In order to evaluate the influence of the nanohybrids surface both on

the internalization efficacy and on the cell cytotoxicity, these nanohybrids have been coated either with (3-aminopropyl)triethoxysilane (APTES) to introduce amine groups on the MPNHs (MPNH-NH_2) or with diglycolic anhydride (DGA) to introduce carboxylic acids functions (MPNH-COOH) (Fig 1.f). The different MPNHs have a spherical-like shape (Fig 1.a-d) and persistent luminescence properties after both UV and visible excitation (Fig 1.e). The light emission can persist for several dozen of minutes after the end of the excitation, which is necessary to get *in vivo* optical signals without background. Figure 1.e also informs about the compared efficacy of UV versus visible illumination. As shown on the corresponding decay curves, the persistent luminescence signal is approximately one log weaker following visible light excitation, in comparison with the signal obtained following UV excitation. Such typical trend regarding the persistent luminescence signal of these MPNHs matches the results demonstrated earlier in several other studies from our group.[31,34] More importantly, the persistent luminescence properties of MPNHs do not vary with the percentage of USPIO (Fig 1.e). As expected, the functionalization procedure has an effect on the zeta potential of the MPNHs: MPNHs-NH_2, with the amino groups, are protonated in mQ water and have positive surface charges, whereas MPNHs-COOH, with the carboxylic acids, have negative zeta potentials (Table 1). In addition, the amount of USPIOs does not seem to have any major impact on the global physicochemical properties of the MPNHs. Notably, all MPNHs display both similar zeta potential, either positive around + 40 mV with MPNHs-NH_2 or negative around – 40 mV with MPNHs-COOH, and hydrodynamic diameters which are rather stable around 190 nm from $MPNH_0$-COOH to $MPNH_3$-COOH.

2.2. *In vitro* cell labelling and toxicity assays

As a cell model we have chosen ECFC, a variety of endothelial progenitors.[32,33] Thus, our objective was to find non-toxic conditions to label ECFC with MPNH and allow *in vivo* cell tracking under magnetic control.

We first assessed the influence of three parameters designated as the type of MPNH, the surface coating (-NH_2 or -COOH) and the incubation time (6 h and 24 h) on the global ECFCs viability. To this end, 10^4 cells deposited in 96-well plates were incubated with increasing amounts of nanoparticles. The Alamar blue test was used to evaluate the cell metabolic activity. As can be observed in Fig 2, the coating has an influence on cell viability. When we look at $MPNH_0$ (nanohybrids with 0% of USPIOs), we can verify that amine-coated MPNHs are more cytotoxic than the carboxylic coated ones (Fig 2.a). This is certainly due to the positive charge of amine-coated MPNHs, leading to a higher cellular uptake as can be seen in the literature.[35,36] This apparent toxicity is even more important when the incubation time increases from 6 to 24 hours. In contrast to particle coating, the amount of USPIOs in MPNH type ($MPNH_{1-3}$) has little influence on the cell viability (Fig 2.a-d). Such absence of effect could be attributed to the fact that USPIOs are incorporated into the core of the silica matrix, therefore not in direct contact with the cells. Moreover, this trend is also in line with previous work in which USPIOs alone are not responsible for any significant cytotoxic effect at these concentrations (< 1mM) on endothelial cells.[37,38] Finally, we observed that the low cytotoxicity of MPNHs-COOH is time independent.

Beside the assessment of cellular metabolic activity by Alamar blue test, a cell proliferation assay was carried out up to 7 days post-labeling. For this purpose, we selected a concentration of MPNHs for which the cell viability with the Alamar blue test was above 80% at 24 h, i.e. 0.25 $mg.mL^{-1}$ (which correspond to 73,5 μg of MPNH per cm^2). As can be seen from Fig 2.e, exposure of ECFC to $MPNH_3$-NH_2 appears to significantly alter the proliferation, as compared to a control group (CT). These results are consistent with our previous observation

using the Alamar blue test. On the other hand, incubation of ECFC with $MPNH_3$-COOH does not alter the proliferation of ECFC even after 7 days of proliferation (Fig 2.e).

2.3. Cellular uptake of nanohybrids and opto-magnetic properties of labelled cells

To determine the cell uptake of the MPNHs, different techniques have been used. Since the MPNHs-COOH are less cytotoxic, a concentration of 73,5 $\mu g.cm^{-2}$ (0.25 mg/mL) for each MPNH-COOH was chosen for subsequent experiments. Transmission electron microscopy (TEM) observations of ECFC (6 h after labelling) principally show intra-endosomal confinement of the different $MPNH_{1-3}$-COOH (Fig. 3.a-c), thus indicating that the low toxicity obtained by Alamar blue and proliferation tests are not the consequence of an absence of MPNHs-COOH internalization. We can also observe that these nanoparticles are internalized in different ways: some MPNHs are observed in small intracellular vesicles, while the majority are clustered in large lysosome-like vesicles. MPNHs isolated in small vesicles probably follow clathrin-dependent endocytosis, as previously shown with silica nanoparticles of about one hundred nanometers.[39]

In order to quantify the amount of MPNHs internalized by the cells, a magnetophoresis experiment was performed with cells labelled under conditions identical to that of the TEM experiment. By exploiting the magnetophoretic mobility of each labelled cell in suspension in a magnetic field gradient, we were able to determine the mass of iron per cell, deduced from the measurements of single cell velocity towards the magnet and cell radius (Fig 3.d).[40] Depending on the initial amount of USPIOs in MPNHs, the average mass of iron per cell approximately varies from 1.7 pg to 3 pg. These results are consistent with previous studies reporting EPC labelling with similar USPIOs, which obtained iron load from 3[27] to 10[37] pg per cell after incubation with iron concentrations of 0.1 or 5 mM. In our case, we used lower

iron concentrations ranging from 0.043 to 0.16 mM (for 0.25 $mg.mL^{-1}$ of $MPNH_1$ and $MPNH_3$, respectively) and USPIO were embedded in the silica matrix. In addition to the mean cellular magnetic load, this assay allows determining the iron mass distribution in the cell population (Figure S1). As MPNHs compositions were previously determined using ICP-MS,[31] we could determine the average mass of MPNHs per cell from the magnetophoresis data (Fig 3.e). Unexpectedly, the data from Figure 3.e indicate that the final amount of MPNHs per cell depends on the type of MPNHs. Indeed, the higher the USPIOs load in MPNHs, the lower the MPNHs uptake within each cell. Cells labelled with $MPNH_2$-COOH contain the same amount of iron as those labelled with $MPNH_3$-COOH (Fig 3.d). Thus, $MPNH_3$ are less internalized than $MPNH_2$ and $MPNH_1$.

After the magnetophoresis experiments, the cells were embedded in an agarose gel ($1.5.10^6$ cells per mL) to be characterized by MRI spectrometry in order to measure both T_1 and T_2 relaxation times (Fig S.2 and 3.f). The presence of USPIOs in cells shows a slight but non-significant influence on T_1-weighted images, and no difference between the T_1 of the gel containing the non-magnetic $MPNH_0$-COOH labelled ECFC when compared to the control (Fig S2). As expected from magnetically labelled cells, the contrast evolution is much more important when looking at T_2-weighted images.[41] The gel containing the non-magnetic $MPNH_0$-COOH labelled cells (dark blue column) displayed a contrast similar to the control gel containing unlabelled ECFC (light blue column), but the gels containing cells labelled with magnetic $MPNH_{1,2,3}$ have a much lower T_2 than the control (Fig 3.f).

Due to the dual imaging properties of PLNPs, the labelled cells can be readily detected through their luminescence emission. We compared the luminescence intensity of cells labelled with the four MPNHs under the same conditions. The gels previously used for the MRI experiment were illuminated with a visible LED and the persistent luminescence was measured (Fig 3.g). After visible illumination, the luminescence of the labelled cells clearly

depends on the type of MPNH used. The more USPIO concentration in MPNHs, the lower is the cell luminescence. These variations in the luminescence emission are well correlated to the different cellular uptake reported before (Fig. 3.e). While $MPNH_3$-COOH labelled cell have similar iron content and magnetophoretic mobility compared to $MPNH_2$-COOH labelled cell, their luminescence is 6 times lower than those labelled with $MPNH_2$-COOH (Fig 3.g) which is in line with the different cell uptake. In addition, despite the higher luminescence intensity of $MPNH_1$-COOH labelled cells, their magnetic resonance detectability and magnetic attraction are very low compared to $MPNH_2$-COOH labelled cells. Therefore, in a trade-off between cellular uptake, luminescence detection, MR detection and magnetophoretic mobility of cells, $MPNH_2$-COOH appears as the best candidate to carry out further *in vivo* dual image-guided and magnetically targeted cellular vectorization experiment.

2.4 Functional properties of labelled cells

For *in vivo* cell-based therapy, labelled progenitor cells should maintain crucial biological properties such as migration and capillary network formation abilities.[38,42-44] Thus, we performed two sets of experiments to evaluate these properties. *In vitro*, the study of cell migration was carried out using a scratch/wound healing assay.[45] We created a wound gap in a MPNH-labelled ECFC monolayer by scratching and monitored their migration towards the gap. The remaining gaps in MPNH treated wells were measured when control scratches had disappeared, around 24 h after their realization. Thus, injured areas were photographed to assess healing in each area. Fig 4.a shows the initial injuries (t_0) and 24 hours later (24 h). The wounds are almost all closed after 24 h. Compared to the untreated control, only cells treated with $MPNH_1$-COOH showed significant decrease in the cell ability to close up the gap (Fig 4.f and 4.k). However, according to magnetophoresis results, $MPNH_1$-COOH are the most

internalized nanoparticles by ECFC among USPIOs containing MPNH. It is then conceivable that the greater internalization of $MPNH_1$-COOH is responsible for the longer gap closing delay. It is worthwhile to precise that these results were obtained when cells were cultured in EGM-2 culture medium with 2 % (v/v) of foetal calf serum. This is necessary to avoid a bias due to cell proliferation: a control with 10 % (v/v) of foetal calf serum showed no difference in the wound healing between control and labelled ECFC (data not shown).

As previously mentioned, ECFC have been shown to possess all the characteristics of endothelial progenitor to promote vascular repair and angiogenesis *in vivo*.[32,33] Evaluating their ability to form vascular structures is one of the most specific ways to assess their ability to stimulate angiogenesis. This was tested *in vitro* by plating cells on constituents mimicking the extracellular matrix called Matrigel. Matrigel stimulates the organization of endothelial cells in networks evoking microvasculature. ECFC were labelled with MPNHs-COOH before seeding on Matrigel for 16 h. Under these experimental conditions, labelled and control ECFC formed extensive tubular network and the labelling process did not affect their properties (Fig 5 and Fig S3). Typical characterizations of tubular structures include the total number of tubes and their mean lengths (Fig 5.f and 5.g, respectively), but it is also possible to evaluate the mean covered area, the number of loops, the total length of the network, the loops mean areas and perimeters, as well as the total branching points (Fig S3.a-f, respectively). As can be seen on the Fig 5 and Fig S3, there is no significant difference between the networks formed by labelled and non-labelled ECFC, regardless of the property under consideration. Similar results have already been reported in the literature using magnetic nanoparticles.[37] Altogether, these results confirm the MPNHs innocuousness regarding ECFC pro-angiogenesis properties.

2.5 Real time dynamic tracking and magnetic manipulation of transplanted cells *in vivo*

As a proof of concept, we carried out *in vivo* experiment to determine whether it was possible to follow the distribution of MPNH-labelled ECFC in real time by luminescence imaging and simultaneously to control their localization by magnetic fields. ECFC were labelled with $MPNH_0$-COOH or $MPNH_2$-COOH under the same conditions to those previously used. 5.10^5 labelled ECFC were pre-illuminated by an orange LED for 5 min and were then injected in the peritoneal cavity of BALB/c mice. A luminescence image was acquired before and after applying a magnet to the right side of each mouse. The ECFC labelled with $MPNH_0$-COOH represent the control group since $MPNH_0$ do not contain USPIOs and therefore do not react to the presence of a magnetic field gradient. To evaluate the influence of the presence of an external magnet on the distribution of ECFC, we monitored the persistent luminescence intensity for twelve minutes throughout five regions of interest along the abdominal cavity (red rectangles, Fig 6.a). When looking at the signal of ECFC labelled with $MPNH_0$-COOH, it can be seen that the luminescence in the mice does not evolve (Fig 6.b) and that the luminescence profile traced as indicated above is stable after applying the magnet against the right flank of the mouse (Fig 6.d). On the contrary, when looking at the signal of $MPNH_2$-COOH labelled ECFC, we observe a significant preferential accumulation with time of the luminescence situated in the right part of the abdomen towards the right flank of the mouse, where the magnet is placed (Fig 6.c). Moreover, the luminescence coming from the left half side of the mice did not change over time, unlike that of the right side. The persistent luminescence signal increases significantly in the closest area to the magnet (Fig 6.e). This graph confirms results from the luminescence images: the signal does not evolve at a distance greater than 2 cm from the magnet. This makes it possible to determine an effective distance of action of the magnet on the $MPNH_2$-COOH labelled ECFC. Furthermore, the most important evolution of the luminescence takes place during the 3 or 4 first minutes of the

experiment, suggesting that once cell sedimentation or tissue adhesion happen, no more cell movement can occur in our experimental conditions.

These first experiments of magnetic cellular vectorization using MPNHs *in vivo* show the possibility to magnetically attract MPNHs-loaded cells injected into the peritoneal cavity and to optically localize them in real-time by luminescence measurements. This study proved, for the first time, the feasibility of using nanoparticles as a tool to magnetically vectorize and concomitantly track cell migration *in vivo* in real-time, without unnecessary sacrifice of the animal. The non-invasive nature of this technique opens access to information regarding cell magnetic vectorization dynamics in living animals. This proof of concept was made possible in our situation because it was realised on mice. As near-infrared luminescence does not have an important penetration depth, its actual potential would be limited to preclinical studies on small animals, per-operative imaging and surface applications (dermatology, gastro-intestinal endoscopy). Another promising enhancement of this technique could be achieved using PLNP emitting in the second near-infrared window (between 1.0 and 1.4 μm), as penetration depth is higher for this wavelength range.

3. Conclusion

Nanoparticles with persistent luminescence and magnetic properties were integrated into nanohybrids in order to label cells of therapeutic interest. In this study, we showed that with such MPNHs, it is possible to define non-toxic labelling conditions, which allow cells tracking in real-time using persistent luminescence. Moreover, this led to signals devoid of autofluorescence and allowed following the injected cells *in vivo* dynamic and attraction with a magnet. Our findings provide a proof-of-concept demonstrating that it is possible to realize real-time optical monitoring of magnetically targeted ECFC *in vitro* and *in vivo* with a good

sensitivity using persistent luminescence. Thus, we postulate that, by applying an appropriate magnetic field gradient, the approach developed in this study could be useful to assess cell targeting to specific locations inside the body for cell-based therapies. This study also suggests the possibility to realize cell retention in the peritoneal cavity using our nanoparticles, which may be interesting for applications such as cancer cell therapies[46] if similar results are further obtained with different kind of therapeutic cells.

4. Experimental section

Chemicals and biologics:

Zinc nitrate hexahydrate (>99%), diglycolic anhydride (>90%) and dimethylhydroxylamine solution (40%) were obtained from Fluka. Gallium oxide (99.999%), chromium (III) nitrate nonahydrate (99.99%) and sodium n-dodecyl sulfate (99%) were purchased from Alfa Aesar. Dimethylformamide (>99.99%) was purchased from SDS. Cetyltrimethylammonium bromide (CTAB, >98%), tetraethyl orthosilicate (TEOS, >98%), iron (II) chloride tetrahydrate, caffeic acid and HCl were purchased from Sigma-Aldrich. Water was purified with a Millipore system (resistivity 18.2 MΩ cm). HBSS and D-PBS were purchased from Dubco.

ECFC isolation, culture and labelling:

Umbilical cord blood collected from consenting mothers was diluted in an equal volume of HBSS, and mononuclear cells were isolated by density-gradient centrifugation using 1.077g.mL^{-1} Histopaque solution (Sigma Chemicals, Saint Quentin Fallavier, France) as described by Bompais et al.[47] CD34+ cells were selected with immunomagnetic beads and the MACS technique (Miltenyi Biotec, Paris, France). They were plated on 0.2% gelatin-coated 24-well plastic culture dishes at a density of 5.10^5 cells/well in endothelial growth

medium (EGM-2, Lonza, Walkersville, MD, USA). After 4 days, non-adherent cells were removed by thorough washing with culture medium. After 10 days of culture, ECFC colonies became visible microscopically. Cells were then detached with trypsin-EDTA (Eurobio, Les Ulis, France) and expanded in EGM-@ on 0.2% gelatin coated plates and grown at 37°C in a humidified 5% CO_2 atmosphere for further use. ECFC were used 25 to 45 days after cord blood processing.

Cell labelling was performed by adding a suspension of MPNHs in EGM-2 culture medium to adherent cells. Cells were incubated at 37°C for different incubation times (6 or 24h) with various MPNH concentrations. Incubation was followed by two washes with MPNH-free D-PBS.

Synthesis and functionalization of the four nanohybrids:

Persistent luminescence nanoparticles ($ZnGa_2O_4:Cr^{3+}$), maghemite ultrasmall iron oxide nanoparticles (γ-Fe_2O_3) and the four types of mesoporous nanohybrides were synthesized as previously described.[31]

The surface functionalization of MPNHs was realized as follow: $MPNH_{0,1,2,3}$-NH_2 nanoparticles were obtained by adding APTES (40 μL) to a suspension of $MPNH_{0,1,2,3}$-OH (10 mg) in DMF (4 mL). The reaction mixture was sonicated for the first 2 minutes using a Branson Ultrasonic Cleaner 1210 and kept under vigorous stirring for 5 hours at RT. Particles were washed from the unreacted APTES by three centrifugation/redispersion steps in DMF. $MPNH_{0,1,2,3}$-COOH were obtained by having DGA (2.7 mg) react with $MPNH_{0,1,2,3}$-NH_2 particles (10 mg) in DMF (4 mL) under vigorous stirring overnight at RT. After washing, $MPNH_{0,1,2,3}$-COOH were dispersed in sterile glucose (5%).

Alamar blue assay:

Before realizing this assay, it is necessary to determine the linearity range of this test.

Growing amounts of cells (nine conditions from 4.10^3 to 2.10^4 cells per well) were seeded in 96-well flat bottom plates (Falcon, Strasbourg, France) and incubated subsequently in complete culture medium, without Alamar Blue reagent for 24 hours and with Alamar Blue for 5 hours. Fluorescence measurements were then realized every hour (λ_{exc} = 530 nm / λ_{em} = 590 nm) with a Tecan Infinite Pro 2000 (Tecan Trading AG, Switzerland). This experiment allowed us to determine efficient conditions for the following cytotoxicity assays.

ECFC were seeded at a density of 10^4 cells per well in 96-well flat-bottom plates and incubated in complete culture medium (EGM-2) for 24 hours. Then, medium was replaced by EGM-2 containing increasing concentrations of MPNH-NH_2 or MPNH-COOH. After 6 or 24 hours, medium was removed and EGM-2 with Alamar Blue reagent (10%, v/v) was added for 4 hours at 37°C. Cell viability is calculated from the measured fluorescence of metabolized Alamar Blue using a Tecan Infinite Pro 2000.

Cell proliferation assay:

ECFC were seeded at a density of 10^3 cells per well in 96-well flat-bottom plates and incubated in complete culture medium overnight. Cells were then exposed 6 h to EGM-2 (control), MPNH-NH_2 or MPNH-COOH suspensions in EGM-2 at the concentration of 0.25 mg.mL^{-1}. Mediums were then removed and three control wells, as well as three MPNH-treated wells, were treated as follow: the supernatants were removed, wells were gently washed using 300 µL of DPBS, cells were treated with 20 µL of trypsin-EDTA for 5 min at 37°C before adding 40 µL of 10% trypan blue (v/v) EGM-2, cells were transferred in an Eppendorf tube and another 20 µL of EGM-2 was used to rince the wells. Cells were then counted on a Malassez cell. This action was repeated over time.

Magnetophoresis:

Cellular uptake was quantified by means of magnetophoresis,[48] which consists of measuring the velocity of labelled cells in a magnetic field gradient of know cartography (magnetic field

*gradient gradB = 18.5 mT.mm^{-1}). The iron mass per cell is calculated from the balance of viscous force ($6\pi\eta R\upsilon$, η being the water viscosity, R the cell radius, υ the cell velocity) and the magnetic force (M*gradB, M being the cell magnetic moment). Measuring, from video analysis, the velocity υ and the radius R of cells migrating toward the magnet, we obtain their magnetic moment or, equivalently, their iron mass m_{Fe}. In addition to the mean cellular magnetic load, this assay allows determining the iron mass distribution in the cell population (n > 87 cells for each incubation condition).*

Optical characterization of cells:

Labelled cells were fixed in Eppendorf tubes containing a low gelling point agarose (BMA Products, USA) solution 3% (w/v) at 38°C, and a concentration of 1.5.10^{6} ECFC.mL^{-1}. Eppendorfs were then illuminated for 5 minutes before signal acquisition. Signal acquisition was carried out using a photon-counting system based on a cooled GaAs intensified charge-coupled device (ICCD) camera (Optima, Biospace, Paris, France).

Magnetic characterization of cells:

The agarose gels were also used to perform MRI measurements. MRI was performed with a dedicated small-animal 4.7 Tesla MR system (Biospec 47/40 USR Bruker), using a quadrature transmit/receive body coil with a 35 mm inner diameter. A 5 mm water reference tube was also inserted. The T2 sequence was used with following parameters: TR = 12 s, 100 TE were done from 9 ms with 9 ms between each, 149 x 85 matrix, 3 slices of 1 mm thickness, resolution 235 x 235 μm and FOV = 3.5 x 2 cm. The T1 sequence was used with following parameters: TE = 11 s, TR = 10 s / 7 s / 4,5 s / 3 s / 1,5 s / 800 ms / 400 ms / 200 ms / 150 ms / 100 ms / 90 ms, 149 x 85 matrix, 3 slices of 1 mm thickness, resolution 235 x 235 μm and FOV = 3.5 x 2 cm.

Scratch test:

Cell migration assays were performed by plating 3.10^5 ECFC on 6-well plates until confluence was reached. Then, the cells were treated with 73.5 $\mu g.cm^{-2}$ (0.25 $mg.mL^{-1}$) of each MPNH-COOH for 6 h. Wells were rinsed with PBS and three wounds were realized in each well using a P200 pipette tip. PBS supernatants were discarded and EGM-2 with 2 or 10 % of serum was added. Wounds widths were measured 24 h after they were realized. The cells were imaged using a Nikon Diaphot inverted contrast microscope. The width of the wounds was quantified using ImageJ. Six width measures were performed on three wounds for each condition.

In vitro tube formation assay:

These experiments were carried out with cells labelled under the same conditions as for the previous experiments (MPNH-COOH, 6 h, 73.5 $\mu g.cm^{-2}$ / 0.25 $mg.mL^{-1}$). At the same time, 48-well plates were coated with 150 μL of growth factor reduced Matrigel. Polymerization of Matrigel was realized at 37°C for 1 h. 4.10^4 control and labelled ECFC were loaded on Matrigel and incubated in EGM-2 for 16 h to allow cellular network structures to fully developp. Cell structures were imaged using a Nikon Diaphot inverted contrast microscope, and networks were characterized with the online software Wimasis Image Analysis, using the Wimtube protocol (www.wimasis.com/en/products/13/WimTube).

In vivo cell imaging and tracking:

Animal studies were conducted in agreement with the French guidelines for animal care in compliance with procedures approved by the Paris Descartes ethics committee for animal research (ref. CEEA34.JS.142.12). Five weeks old female BALB/c mice (Janvier, Le Genest St. Isle, France) were anesthetized by oral inhalation of isoflurane. A quantity of 5.10^5 ECFC were labelled with either $MPNH_0$-COOH (control) or $MPNH_2$-COOH under previously determined conditions (6 h, 73.5 $\mu g.cm^{-2}$ / 0.25 $mg.mL^{-1}$). These ECFC were dispersed in 100

μL of a 5% sterile D-PBS solution at a concentration of 5.10^6 ECFC.mL^{-1}. The suspension of labelled ECFC was first excited ex vivo for 5 minutes under an orange LED before injection in the peritoneal cavity of mice. Animals were then placed on their back under the photon-counting device, and the signal acquisitions were performed. A luminescence image was realized for ten seconds before applying a magnet against the right side of the mouse. Luminescence was then followed for ten minutes, until its distribution stops evolving. Four ring neodymium magnets (outer diameter 19.1 mm, inner diameter 9.5 mm, height 6.4 mm, strength 75.5 N, Supermagnete, Gottmadingen, Germany) were joined to be applied on the side of the mouse.

Acknowledgements

The authors sincerely thank Anna Lokajczyk and Nour Bacha for their advices and help concerning ECFC cultures and experiments (from the laboratory "Therapeutiques innovantes en hémostase", Inserm U S1140), Johanne Seguin (from the UTCBS, CNRS UMR 8258), René Lai-Kuen and Bruno Saubaméa (from the technological Platform of IFR71/IMTCE-Cellular & Molecular Imaging), Dan Elgrabli (from the MSC, CNRS UMR 7057), as well as Florence Delestre and Maurice Teston for their unwavering support. This work was supported by a grant from the Pres Sorbonne Paris-Cité (ODICEO project).

References

[1] A. Trounson, C. McDonald, Cell Stem Cell **2015**, *17*, 11.

[2] N.J. Leeper, A.L. Hunter, J.P. Cooke, Circulation **2010**, *122*, 517.

[3] R.J. Morris, Y. Liu, L. Marles, Z. Yang, C. Trempus, S. Li, J. S. Lin, J. A. Sawicki and G. Cotsarelis, Nat. Biotechnol. **2004**, *22*, 411.

[4] W.-B. Shen, C. Plachez, O. Tsymbalyuk, N. Tsymbalyuk, S. Xu, A. Smith, S. Michel, D. Yarnell, R. Mullins, R. Gulapalli, A. Puche, J.M. Simard, P.S. Fishman and P. Yarowsky, Cell Transplant. **2016**, *25*, 1085.

[5] M. Ishii, Y. Numaguchi, K. Okumura, R. Kubota, X. Ma, R. Murakami, K. Naruse, T. Murohara, Atherosclerosis **2009**, *206*, 109.

[6] F. Zemani, J.-S. Sylvestre, F. Fauvel-Lafeve, A. Bruel, J. Vilar, I. Bieche, I. Laurendeau, I. Galy-Fauroux, A.-M. Fischer, C. Boisson-Vidal, Arterioscler. Thromb. Vasc. Biol. **2008**, *28*(4), 644.

[7] I.M. Barbash, P. Chouraqui, J. Baron, M.S. Feinberg, S. Etzion, A. Tessone, L. Miller, E. Guetta, D. Zipori, L.H. Kedes, R.A. Kloner, J. Leor , Circulation **2003**, *108*, 863.

[8] D.J. Brenner, E.J. Hall, N. Engl. J. Med. **2007**, *357*, 2277.

[9] M. Modo, J. Kolosnjaj-Tabi, F. Nicholls, W. Ling, C. Wilhelm, O. Debarge, F. Gazeau, O. Clement, Contrast Media Mol. Imaging **2013**, *8*, 439.

[10] C. Yoshida, A.B. Tsuji, H. Sudo, A. Sugyo, C. Sogawa, N. Inubushi, T. Uehara, T. Fukumura, M. Koizumi, Y. Arano, T. Saga, Nucl. Med. Biol. **2011**, *38*, 331.

[11] J.L. Ortiz, A. Ortiz, J. Milara, M. Armengot, C. Sanz, D. Compan, E. Morcillo, J. Cortijo. Plos One **2016**, 11, e0164399.

[12] J. Li, W.Y. Lee, T. Wu, J. Xu, K. Zhang, G. Li, J. Xia, L. Bian. Adv. Helthcare Mater. **2016**, *77*, 14.

[13] H. Yukawa, S. Mizufune, C. Mamori, Y. Kagami, K. Oishi, N. Kaji, Y. Okamoto, M. Takeshi, H. Noguchi, Y. Baba, M. Hamaguchi, N. Hamajima, S. Hayashi, Cell Transplant. **2009**, *18*, 591.

[14] H. Yukawa, M. Watanabe, N. Kaji, Y. Baba, Cell Med. **2014**, *7*, 75.

[15] Q. le Masne de Chermont, C. Chanéac, J. Seguin, F. Pellé, S. Maîtrejean, J.-P. Jolivet, D. Gourier, M. Bessodes, D. Scherman, Proc. Natl. Acad. Sci. USA **2007**, *104*, 9266.

[16] T. Maldiney, A. Lecointre, B. Viana, A. Bessiere, M. Bessodes, D. Gourier, C. Richard, D. Scherman, J. Am. Chem. Soc. **2011**, *133*, 11810.

[17] T. Maldiney, B. Viana, A. Bessiere, D. Gourier, M. Bessodes, D. Scherman, C. Richard, Opt. Mater. **2013**, *35*, 1852.

[18] T. Maldiney, A. Bessière, J. Seguin, E. Teston, S.K. Sharma, B. Viana, A.J.J. Bos, P. Dorenbos, M. Bessodes, D. Gourier, D. Scherman, C. Richard, Nat. Mater. **2014**, *13*, 418.

[19] T. Lécuyer, E. Teston, G. Ramirez-Garcia, T. Maldiney, B. Viana, J. Seguin, N. Mignet, D. Scherman, C. Richard, Theranostics **2016**, *6*, 2488.

[20] E. Teston, S. Richard, T. Maldiney, N. Lièvre, G. Yangshu Wang, L. Motte, C. Richard, Y. Lalatonne, Chem. Eur. J. **2015**, *21*, 7350.

[21] S.-Q. Wu, C.-W. Chi, C.-X. Yang, X.-P. Yan, Anal. Chem. **2016**, *88*, 4114.

[22] S.-Q. Wu, C.-X. Yang, X.-P.Yan. Adv. Funct. Mater. **2017**, 1604992.

[23] S.K. Sanganalmath, R. Bolli, Circ. Res. **2013**, *113*, 810.

[24] G. Vunjak-Novakovic, K.O. Lui, N. Tandon, K.R. Chien, Annu. Rev. Biomed. Eng. **2011**, *13*, 245.

[25] B. Polyak, I. Fishbein, M. Chorny, I. Alferiev, D. Williams, B. Yellen, G. Friedman, R. J. Levy, Proc. Natl. Acad. Sci. USA **2008**, *105*,698.

[26] L. Cheng, C. Wang, X. Ma, Q. Wang, Y. Cheng, H. Wang, Y. Li, Z. Liu, Adv. Funct. Mater. **2013**, *23*, 272.

[27] A. Chaudeurge, C. Wilhelm, A. Chen-Tournoux, F. Farahmand, V. Bellamy, G. Autret, C. Ménager, A. Hagège, J. Larghéro, F. Gazeau, O. Clément, P. Menasché, Cell Transplant. **2012**, *21*, 679.

[28] J. Riegler, A. Liew, S.O. Hynes, D. Ortega, T. O'Brien, R.M. Day, T. Richards, F. Sharif, Q.A. Pankhurst, M.F. Lythgoe, Biomaterials **2013**, *34*(8),1987.

[29] B. Polyak, M. Medved, N. Lazareva, L. Steele, T. Patel, A. Rai, M.Y. Rotenberg, K. Wasko, A.R. Kohut, R. Sensenig, G. Friedman, ACS Nano, **2016**, *10*(10), 9559.

[30] B. Polyak, I. Fishbein, M. Chorny, I. Alferiev, D. Williams, B. Yellen, G. Friedman, R.J. Levy. Proc. Natl. Acad. Sci. USA. **2008**, *105*(2), 698.

[31] E. Teston, Y. Lalatonne, D. Elgrabli, G. Autret, L. Motte, F. Gazeau, D. Scherman, O. Clément, C. Richard, T. Maldiney, Small **2015**, *11*, 2696.

[32] M.C. Yoder, L.E. Mead, D. Prater, T.R. Krier, K.N. Mroueh, F. Li, R. Krasich, C.J. Temm, J.T. Prchal, D.A.Ingram, Blood **2007**, *109*(5), 1801.

[33] C. Bouvard, B. Gafsou, B. Dizier, I. Galy-Fauroux, A. Lokajczyk, C. Boisson-Vidal, A.-M. Fischer, D. Helley, Arterioscler. Thromb. Vasc. Biol. **2010**, *30*, 1569.

[34] T. Maldiney, B. Ballet, M. Bessodes, D. Scherman, C. Richard, Nanoscale **2014**, *6*, 13970.

[35] A.M. Abdelmonem, B. Pelaz, K. Kantner, N.C. Bigall, P. del Pino, W.J. Parak, J. Inorg. Biochem. **2015**, *153*, 334.

[36] T.-H. Chung, S.-H. Wu, M. Yao, C.-H. Lu, Y.-S. Lin, Y. Hung, C.-Y. Mou, Y.-C. Chen, D.-M. Huang, Biomaterials, **2007**, *28*(19), 2959.

[37] C. Wilhelm, L. Bal, P. Smirnov, I. Galy-Fauroux, O. Clément, F. Gazeau, J. Emerich, Biomaterials **2007**, *28*, 3797.

[38] Z. Orynbayeva, R. Sensenig, B. Polyak. Nanomedicine (Lond). **2015**, *10*(10), 1555.

[39] D.-M. Huang, Y. Hung, B.-S. Ko, S.-C. Hsu, W.-H. Chen, C.-L. Chien, C.-P. Tsai, C.-T. Kuo, J.-C. Kang, C.-S. Yang, C.-Y. Mou, Y.-C. Chen, FASEB J. **2005**, *19*, 2014.

[40] J. Kolosnjaj-Tabi, C. Wilhelm, O. Clément, F. Gazeau, J. Nanobiotechnology **2013**, *11*(Suppl 1):S7.

[41] M. Levy, C. Wilhelm, M. Devaud, P. Levitz, F. Gazeau, Contrast Media Mol. Imaging **2012**, *7*(4), 373.

[42] F. Gazeau, C. Wilhelm, Future Medicinal Chemistry, **2010**, *2*(3), 397.

[43] J. Emmerich, Int. J. Low Extrem. Wounds, **2005**, *4*(4), 234.

[44] H. Lawall, P. Bramlage, B. Amann, J. Vasc. Surg. **2011**, *53*(2), 445.

[45] C. C. Liang, A. Y. Park, J. L. Guan, Nat. Protoc. **2007**, *2*, 329.

[46] S. C. Katz, G. R. Point, M. Cunetta, M. Thorn, P. Guja, N. J. Espat, C. Boutros, N. Hanna, R. P. Junghans, Cancer Gene Ther. **2016**, *23*(5), 142.

[47] H. Bompais, J. Chagraoui, X. Canron, M. Crisan, X.H. Liu, A. Anjo, C. Tolla-Le Port, M. Leboeuf, P. Charbord, A. Bikfalvi, G. Uzan, Blood, **2004**, *103*(7), 2577.

[48] C. Wilhelm, F. Gazeau, J.C. Bacri, Eur. Biophys. J. **2002**, *31*(2), 118.

Figures

Figure 1: TEM images of non-functionalized $MPNH_0$ (a), $MPNH_1$ (b), $MPNH_2$ (c), $MPNH_3$ (d). e) Decay curves of MPNHs after 2 min UV (254 nm) or red-LED illumination Persistent luminescence intensity is expressed in log_{10} scale in arbitrary units. f) Synthetic pathway from MPNHs-OH to MPNHs-COOH. (adapted from [31])

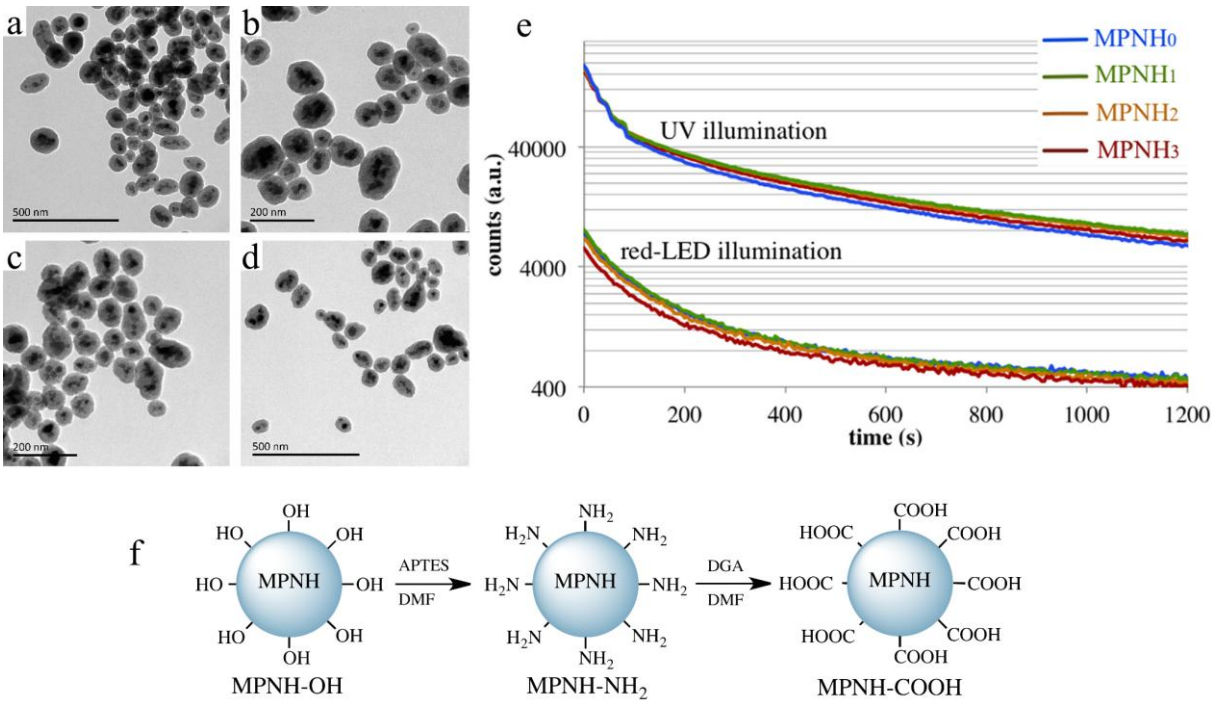

Figure 2: Cytotoxicity of MPNHs in ECFC. a-d) Percentage of viability after 6 (red and blue diamonds) or 24 h (black squares) of incubation with MPNHs-NH_2 (red curves) or MPNHs-COOH (blue curves). All types of MPNH ($MPNH_0$ to $MPNH_3$, as shown on graphs (a) to (d), respectively) were tested for concentrations from 31.25 $\mu g.mL^{-1}$ (9.19 $\mu g.cm^{-2}$) to 1 $mg.mL^{-1}$

(294 µg.cm^{-2}). e) Cell proliferation after incubation in the absence (control, blue diamonds) or presence of MPNH$_3$-NH$_2$ (red squares) or -COOH (green squares) (incubation time 6 h, concentration of 0.25 mg.mL^{-1} / 73.5 µg.cm^{-2}). Growth capacity was not affected by the carboxylic coating, as opposed to the amino coating, compared with growth capacity in control.

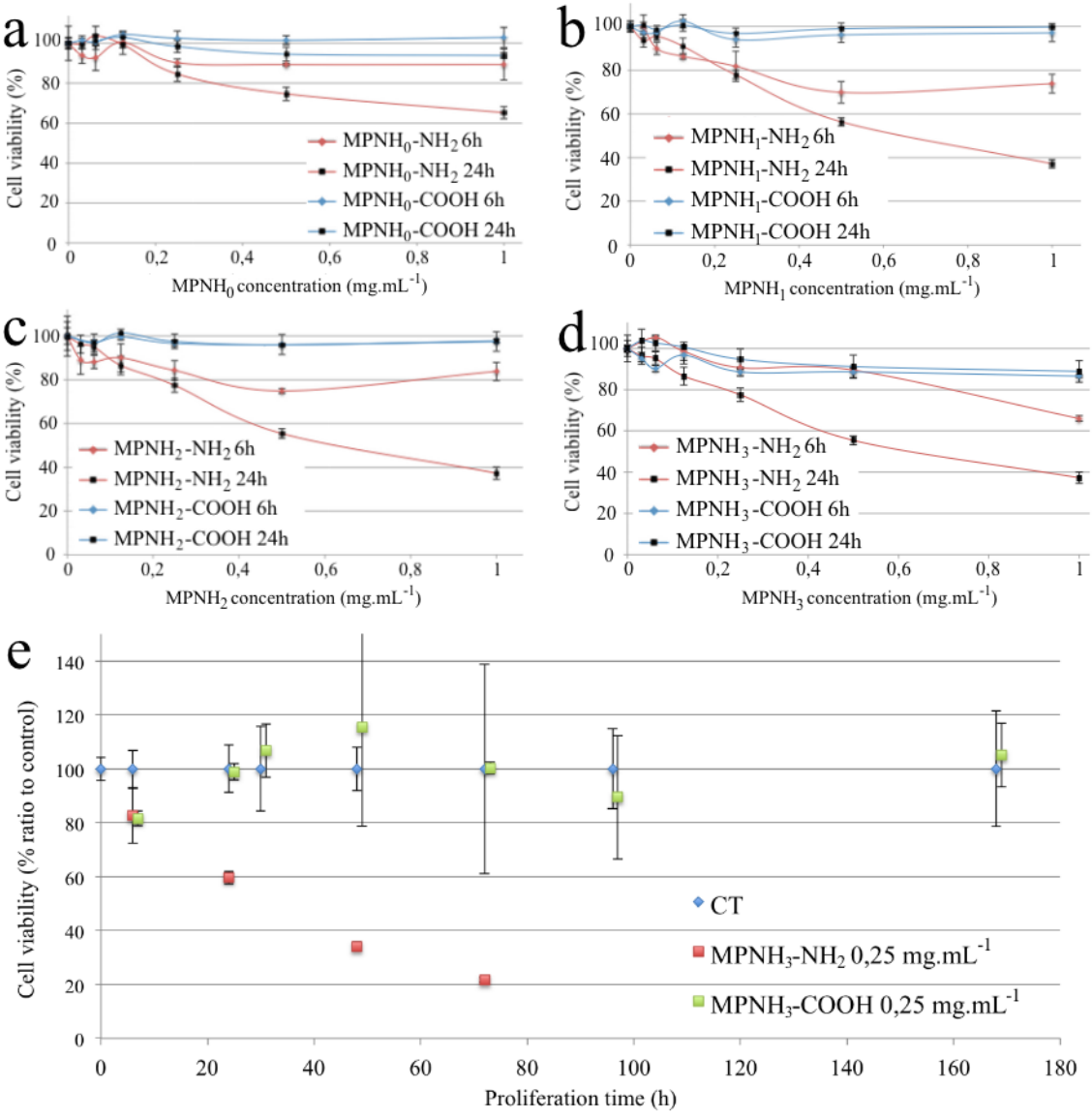

Figure 3: Optical and magnetic characterizations of MPNHs labelled ECFC. a-c) Electron micrographs of ECFC after 6 h of incubation with MPNH$_1$-COOH (a), MPNH$_2$-COOH (b) and MPNH$_3$-COOH (c) (0.25 mg.mL^{-1} / 73.5 µg.cm^{-2}). Fe (d) and MPNH$_{1,2,3}$-COOH (e) mean

load per cell after incubation. Statistical analyses were realized using an Anova test followed by a Bonferroni comparison. Bar graphs show mean ± SEM (n = 88, 178 and 109 for $MPNH_1$, $MPNH_2$ and $MPNH_3$, respectively). ** and *** correspond to $p < 0.01$ and 0.001, respectively. f) T_2* MRI measurements and images of agarose gels with $1.5.10^6$ ECFC.mL^{-1}. Control tube (CT, sky blue) contains the same concentration of unlabelled ECFC. Bar graph show mean ± SD, images of corresponding tubes are shown under the graphics. g) Persistent luminescence of previously described agarose gels after 5 min of red-LED illumination (bar graph show mean ± SD).

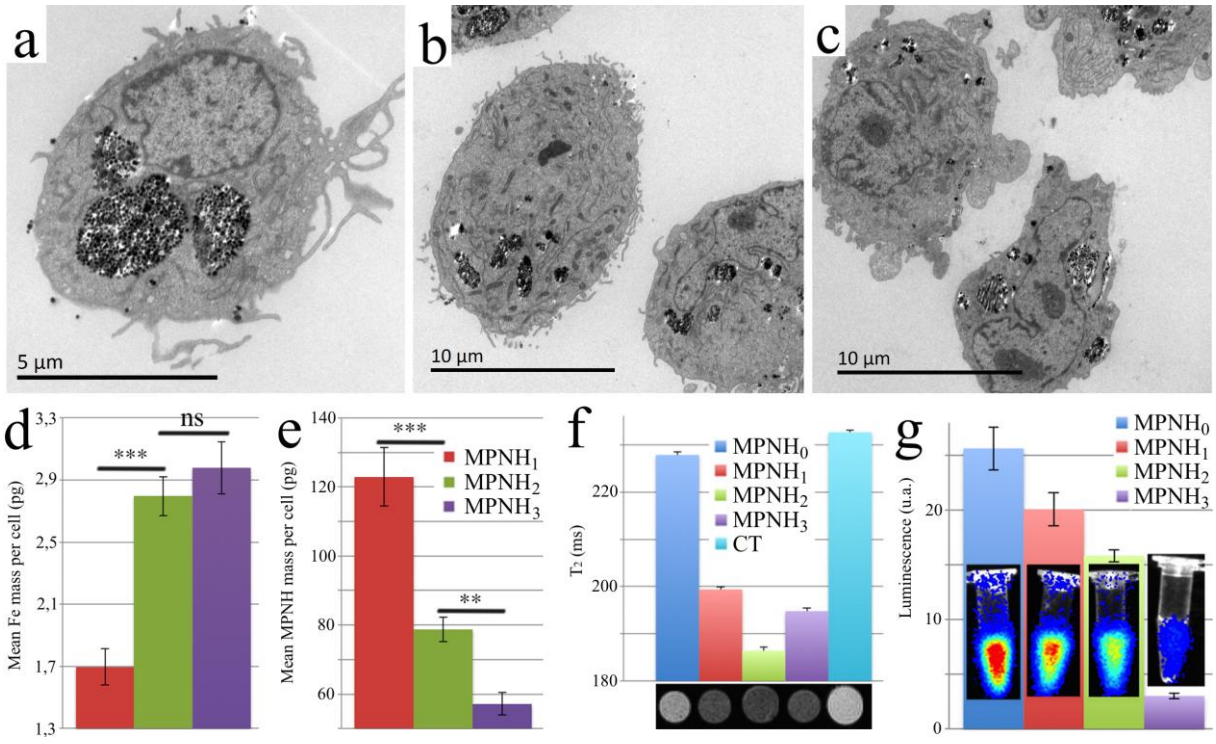

Figure 4: Assessment of the invasion ability of labelled ECFC. a-j) Images of wounds were taken 24 h after their realization, when control wounds have disappeared. k) Evaluation of invasion latency between control and labelled ECFC. Statistical analyses were realized using

an Anova test followed by a Bonferroni comparison. Bar graphs show mean bar graph show mean ± SD, * indicates $p < 0.05$.

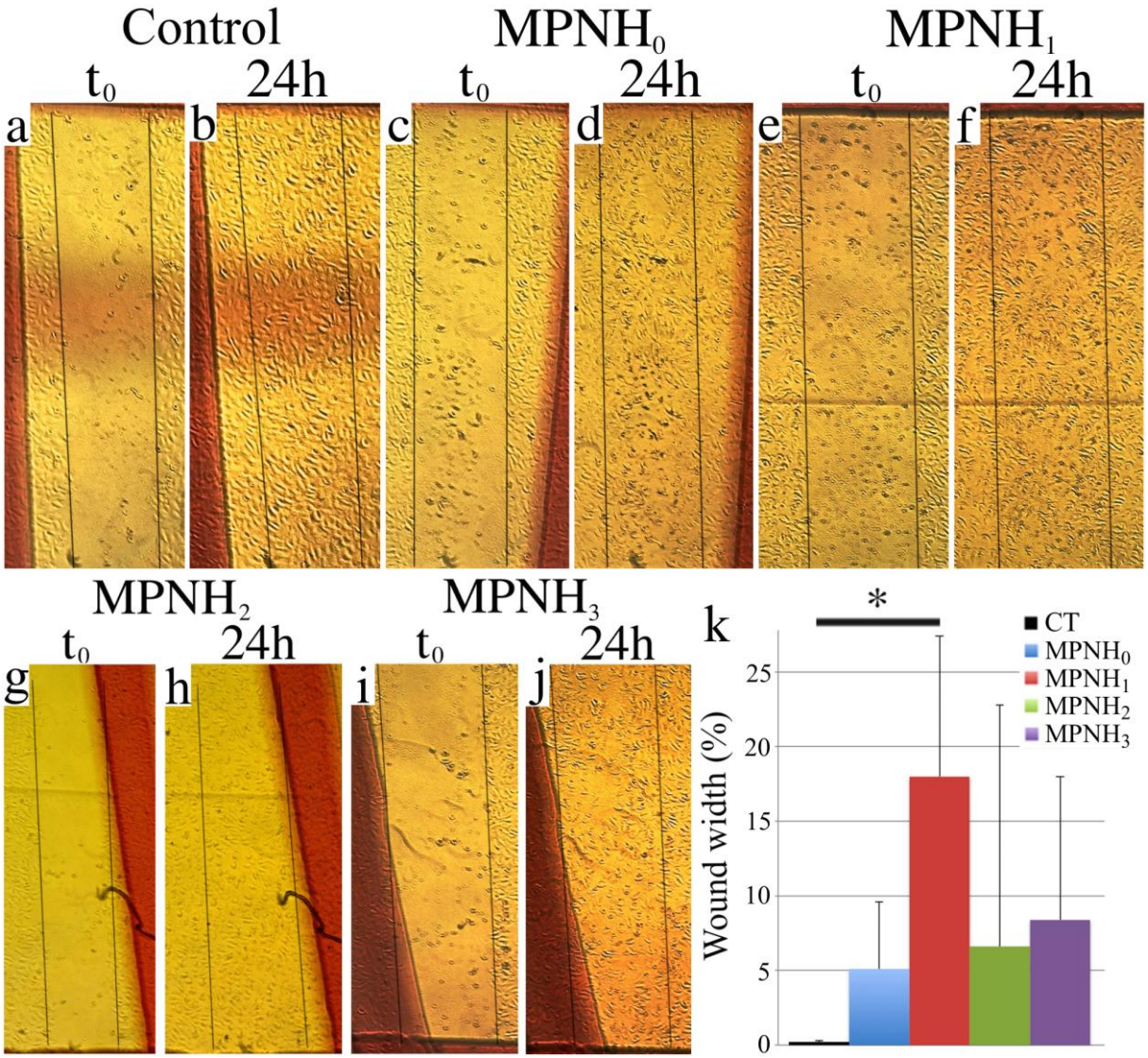

Figure 5: Vasculogenesis *in vitro* with labelled cells on Matrigel. Control (a) and $MPNH_{0,1,2,3}$-COOH (respectively b, c, d and e) labelled ECFC were incubated at 37°C in EGM-2 during 16 h to form vascular tubes. f-g) Properties of the vascular network such as the total number

of tubes (f) or the mean tube length (g) were assessed with an online software (Wimasis). Bar graphs represent mean ± SD.

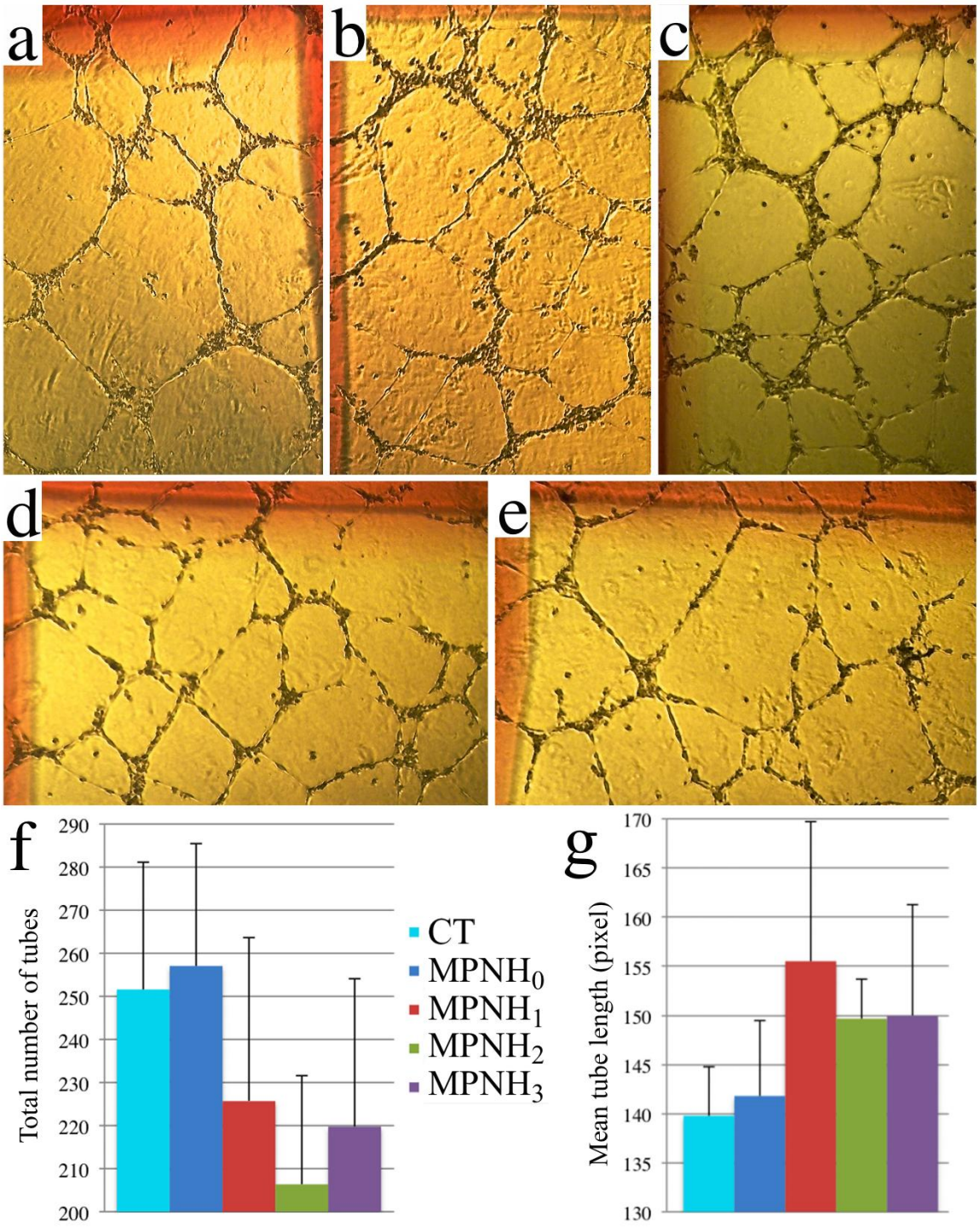

Figure 6: *In vivo* magnetic vectorisation of labelled ECFC and real-time optical imaging of their biodistribution. a) Representation of the *in vivo* experiment and segmentation of mice abdomen to follow the evolution of the luminescence distribution. b-e) Caracteristic evolution of persistent luminescence distribution in a mouse after injection of $MPNH_0$-COOH labelled ECFC (b, control experiment) or $MPNH_2$-COOH labelled ECFC (c) and corresponding graphs (respectively d and e). Statistical analyses were realised between the luminescence intensities before and 12 min after magnet apposition using an Anova test followed by a Bonferroni comparison. * and *** indicate $p < 0.05$ and $p < 0.001$.

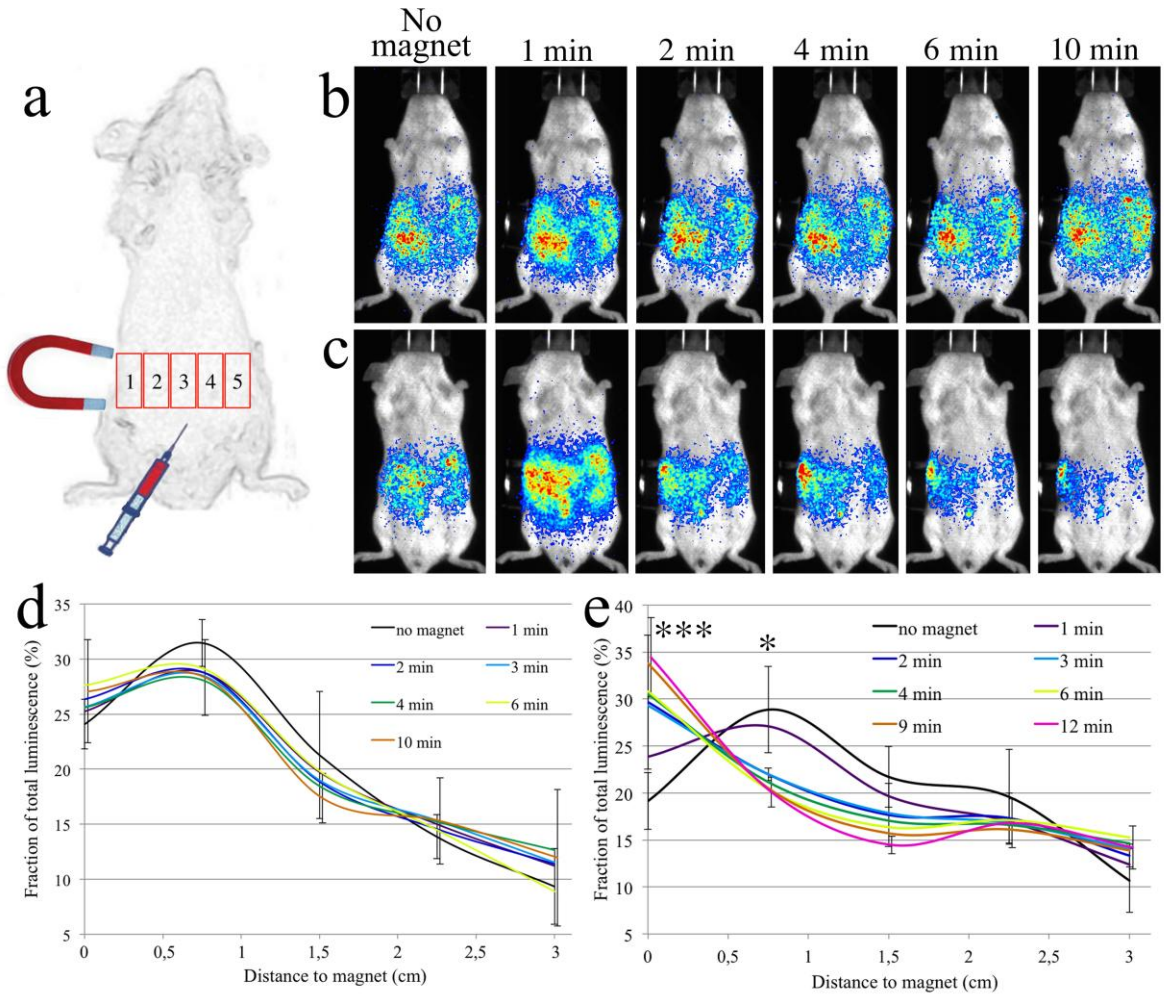

Tables

Table 1: DLS measurements giving hydrodynamic diameters and ζ-potentials of MPNHs-NH_2 and MPNHs-COOH.

	Potentiel ζ (mV)		**Hydrodynamic Diameter (nm) / Polydispersity index**	**Potentiel ζ (mV)**
$MPNH_0$-NH2	36,2 ± 1,9	**$MPNH_0$-COOH**	200 / 0,024	-44,7 ± 2,1
$MPNH_1$-NH2	38,3 ± 0,9	**$MPNH_1$-COOH**	185 / 0,046	-42,2 ± 2,1
$MPNH_2$-NH2	46,3 ± 2,4	**$MPNH_2$-COOH**	191 / 0,050	-39,2 ± 2,2
$MPNH_3$-NH2	35,7 ± 2,7	**$MPNH_3$-COOH**	186 / 0,052	-40,0 ± 2,6

Supplementary

Figure S1: Iron mass distribution in MPNHs-COOH labelled ECFC. a) $MPNH_0$-COOH, b) $MPNH_2$-COOH, c) $MPNH_3$-COOH.

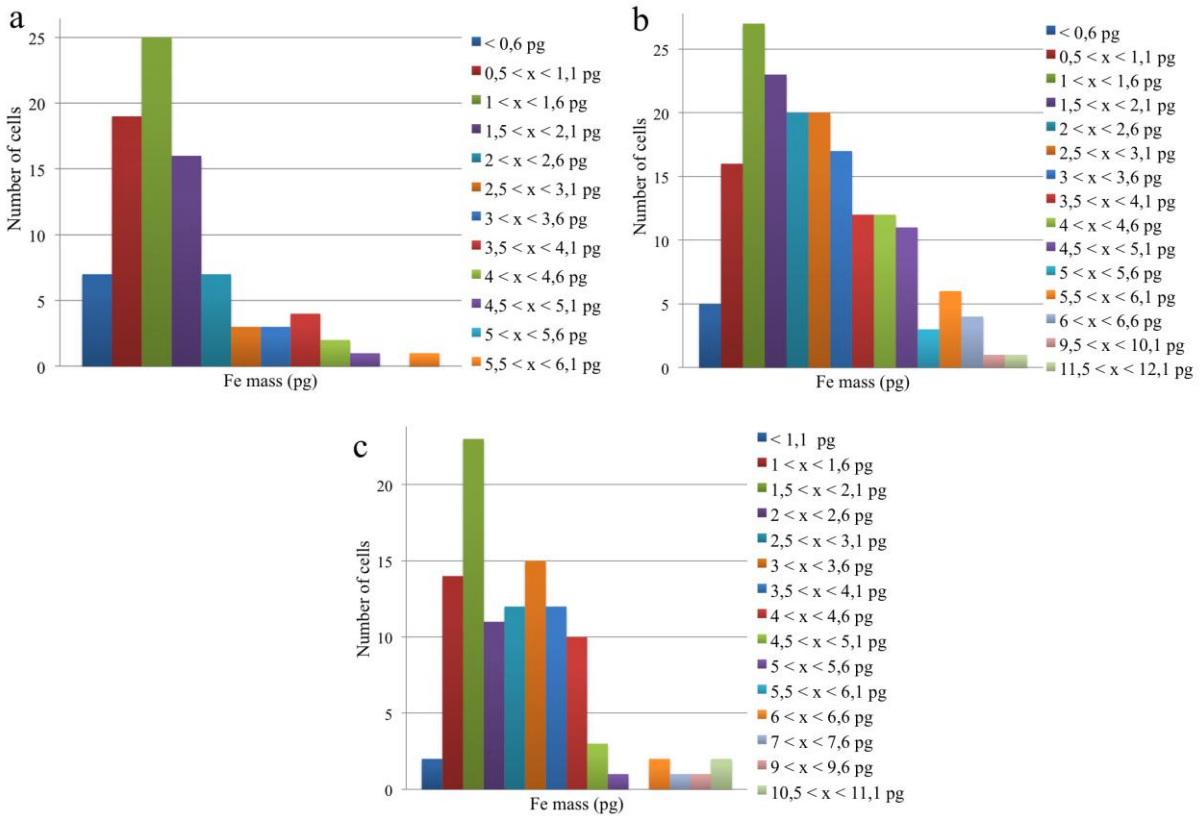

Figure S2: T_1* MRI measurements and images of agarose gels with $1.5.10^6$ ECFC.mL^{-1}. Control tube (CT, sky blue) contains the same concentration of unlabelled ECFC. Bar graph show mean ± SD, images of corresponding tubes are shown under the graphics.

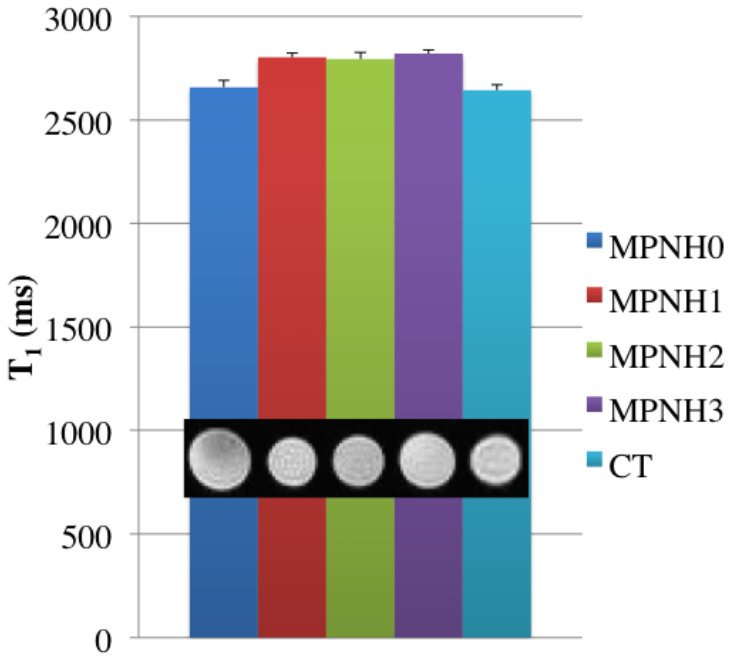

Figure S3: Supplementary characterizations of vascular network formed by unlabelled and MPNHs-COOH labelled ECFC deposited on Matrigel.

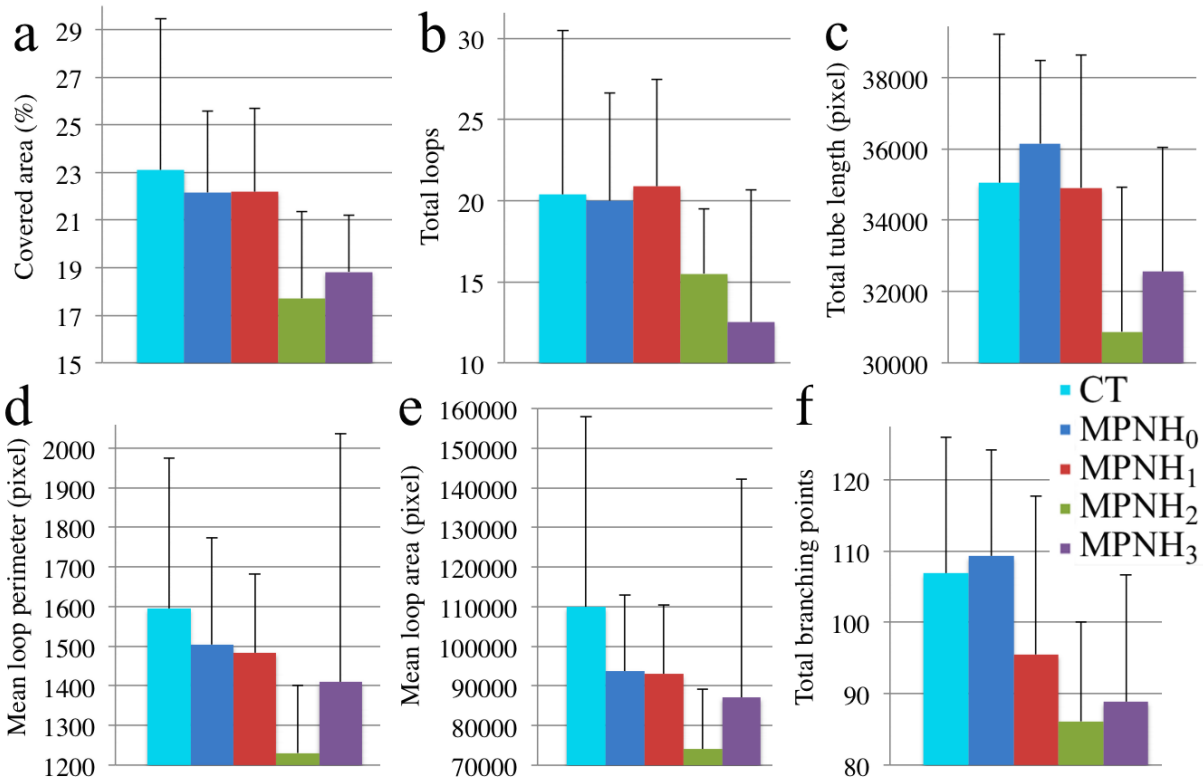
a
Covered area (%)
29
27
25
23
21
19
17
15
b
Total loops
30
25
20
15
10
c
Total tube length (pixel)
38000
36000
34000
32000
30000
d
Mean loop perimeter (pixel)
2000
1900
1800
1700
1600
1500
1400
1300
1200
e
Mean loop area (pixel)
160000
150000
140000
130000
120000
110000
100000
90000
80000
70000
f
Total branching points
120
110
100
90
80
CT
MPNH0
MPNH1
MPNH2
MPNH3